Ecological Engineering & Environmental Technology, 2025, 26(12), 139–157 https://doi.org/10.12912/27197050/214095 ISSN 2719–7050, License CC-BY 4.0

Assessment of the impact of Amizour's mineral deposits associated with Miocene igneous rocks on groundwater quality in the Soummam basin, Algeria

Mahmoud Zaidi^{1*}, Abdelhamid Saou¹, Mustapha Maza¹, Sabrina Bendouma², Farid Ait Merzeg^{3,4}

- ¹ Applied Hydraulics and Environment Research Laboratory, Faculty of Technology, Abderahmene Mira University, Bejaia 06000, Algeria
- ² Earth Sciences Faculty, Mining Department, Badji Mokhtar University Annaba 23000, Algeria
- ³ Scientific and Technical Research Center in Physical and Chemical Analyses (CRAPC), BP384 Bou-Ismail, RP 42004 Tipaza, Algeria
- ⁴ Technical Platform for Physico-chemical Analyzes (PTAPC-Bejaia), Targa Ouzemmour, 06000 Bejaia, Algeria
- * Corresponding author's e-mail: mahmoud.zaidi@univ-bejaia.dz

ABSTRACT

Water and mineral resources are of paramount importance for the economic and social development of any country. Algeria is among the countries facing a critical level of water stress, which exerts environmental pressure on decision-making for water supply development projects and poses a significant challenge to achieving the sustainable development goals (SDGs). The Amizour deposits is recognized as one of the world's largest deposits, however its proximity to the Soummam aquifer raises concerns about the environmental impact of its upcoming mining operations. In this study, a hydrochemical analysis was conducted to assess the impact of the Amizour deposits on groundwater quality. Twenty-six (26) samples were collected during the low-water period and twenty-two (22) during the high-water period, in accordance with international standards organization (ISO) 5667 standards. Geographic information system (GIS) software was used to analyze the spatial and temporal distribution of physico-chemical parameters. Gibbs diagrams, Pearson correlation matrices, and principal component analysis (PCA) were applied to identify the mechanisms controlling water quality, determine the contributing factors to the hydrochemical composition, and classify the different types and sources of pollution. The results reveal a co-occurrence of both geogenic and anthropogenic pollution in Amizour's groundwater, with high concentrations of iron, lead, Manganese, and Zinc reaching 17.75 mg/L, 6.99 mg/L, 6.46 mg/L, and 4.74 mg/L, respectively.

Keywords: water resources, water stress, groundwater quality, hydro chemical analysis, Amizour deposits, geogenic and anthropogenic pollution.

INTRODUCTION

Groundwater interaction is a paramount part of the hydrogeological cycle, essentially controlled by natural processes between water and rock formations. However, quantitative investigations have only recently begun to shed light on the hydrodynamic mechanisms controlling these interactions. As the water infiltrates into the ground, it carries several soluble and insoluble substances that change its quality and alter its

properties (Hartman et al., 2014). Several physic-chemical and biological parameters and their interaction with each other define the water quality (Vasistha et al., 2020) these parametric values show the current state of the water body and therefore show the hydrogeological changes that may affects it over time (Thitame and Pondhe, 2010). These interactions are inherently complex in mineralized rocks, where several mechanisms such as weathering, mineral dissolution, and ion exchange lead to the release of major and trace

Received: 2025.10.24

Accepted: 2025.11.15

Published: 2025.12.01

elements from host rocks into groundwater, thereby altering groundwater chemistry. Understanding these processes is important for identifying the origin of contaminants, whether anthropogenic or geogenic especially in regions with mineralized formations.

Recent studies have highlighted the importance of evaluating groundwater in mineralized regions to distinguish pollution sources, identify the contaminants responsible, and establish appropriate mitigation plans to avoid further deterioration of groundwater quality. Mineralized and mining zones worldwide are known as major sources of groundwater pollution, thus, Numerous studies conducted in various geological formations in North America (Chaillou et al., 2017) Asia (Singha et al., 2022; Kumar and Krishnaa, 2021; Li et al, 2022; Rashid et al., 2023; Hao et al.,2024), Europe (Medunić et al., 2020) and Africa (Smida et al., 2022; Olalekan et al., 2023) have systematically focused on the quality of groundwater and its interactions with surrounding mineralized formations. In Algeria, groundwater is a main source of drinking water supply due to water stress and drought in many areas (Fares et al., 2021), thus, several studies have focused on groundwater quality by evaluating heavy metal concentrations caused by geogenic pollution (Saadali et al., 2022; Barkat et al., 2023).

Numerous investigations have been conducted on Soummam groundwater, and various researcher have highlighted different source of contamination. Saadali and Dadachi (2023) identified the existence of three vulnerability zones: medium, high, very high - using the DRASTIC and SINTACS methodologies, while assessing Cd, Pb and Zn pollution in the upstream part of the present study area. Moreover, Kessasra et al. (2021) reported that both excessive pumping and high levels of dissolved chlorides contributed to the pollution of alluvial aquifer of Lower Soummam. In addition, Saou et al. (2012) observed that the water becomes sodic chlorated from Oued Ghir to the sea, and attributed the high salt content to the marine. Finally, Ouyahia et al. (2024), by combining hydrogeochemical tracking and differential gauging, emphasized the dominance of the geological and hydrogeological environment, which supports the low Sommam aquifers recharge by the tributaries of the slopes that contain evaporitic Triassic formations and a Miocene-aged limestone.

Despite extensive research on anthropogenic heavy metals contamination, double salinization processes, and the effects of gypsum-bearing formations in the Soummam region, the influence of Amizour's igneous rocks and their associated mineralization to groundwater quality remains unexplored. To address this gap, the present study combines multivariate statistical analysis and spatial distribution of physicochemical parameters of groundwater samples to evaluate the relationship and interactions between the Amizour mineral deposits and the Soummam groundwater.

MATERIALS AND METHODS

Study area description

The Amizour valley is located in the northern part of the Soummam Watershed (Figure 1), geographically between longitudes 4°54 E to 5°3 E and latitudes 36°37 N to 36°43 N. It is situated on the right side of Oued Soummam and it is bounded to the West by the Amizour River, to the East by the Bejaia Gulf, and to the South by the Soummam watershed limits. The region is distinguished by the Miocene volcano-plutonic massif, which appertain to the Maghrebides Tertiary magmatic rocks. The study area is distinguished by a humid Mediterranean climate with a monthly average temperature reaching 25.6 °C from June to September. In contrast, the winter months have the lowest temperatures of 11.4 °C. The rainfall ranges from 10.6 mm in July to 113 in in February (Benabbes et al., 2024), with a yearly average of 750 mm (Saou et al., 2012). The area's topographic map (Figure 2) shows elevations of up to 900 meters.

Several researchers (Leikine and Semroud, 1988; Assanaliev et al., 1984). focused on geological, hydrogeological and structural investigations in study area which is consisted of both igneous and sedimentary rocks, stratified from Triassic to quaternary period (Figure 3). Mesozoic formations include Triassic, Jurassic and cretaceous. The Triassic indicates Gypsumsaline facies and occur with versicolored marls, dolomites and Cornieule, the middle and upper Jurassic are composed of red sandstones, puddingstones, and micaceous sandstones, whereas the lower Jurassic is composed of marly limestones, limestones and silicate-conglomerate rocks. While all of the lower, middle, and upper Cretaceous occurs in the Soummam valley, only

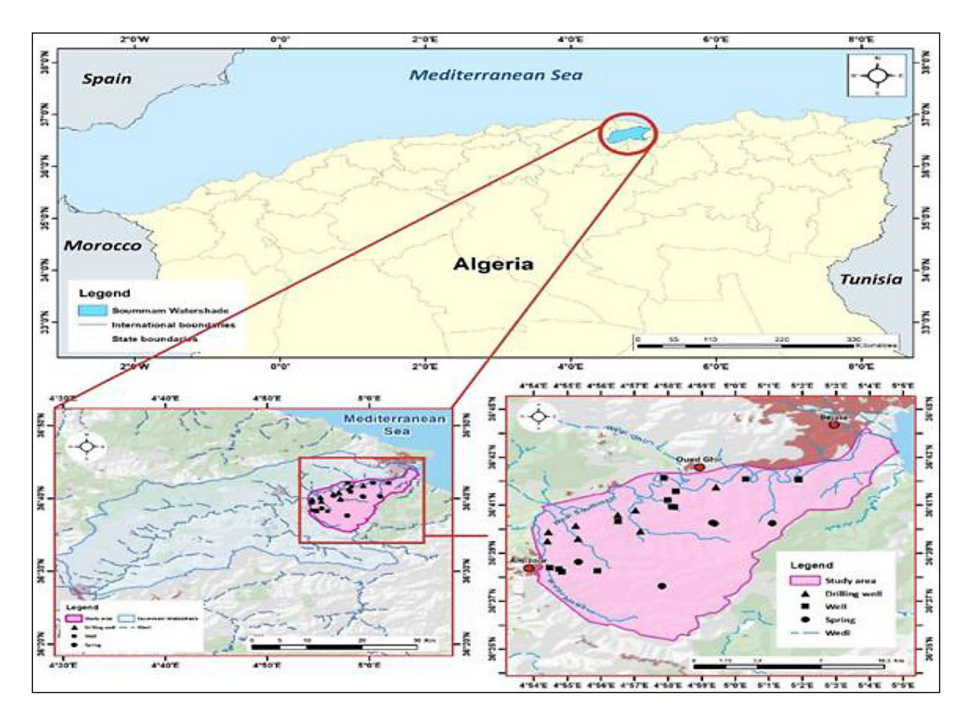


Figure 1. The Soummam watershed's and the study region's (Amizour) geographic location

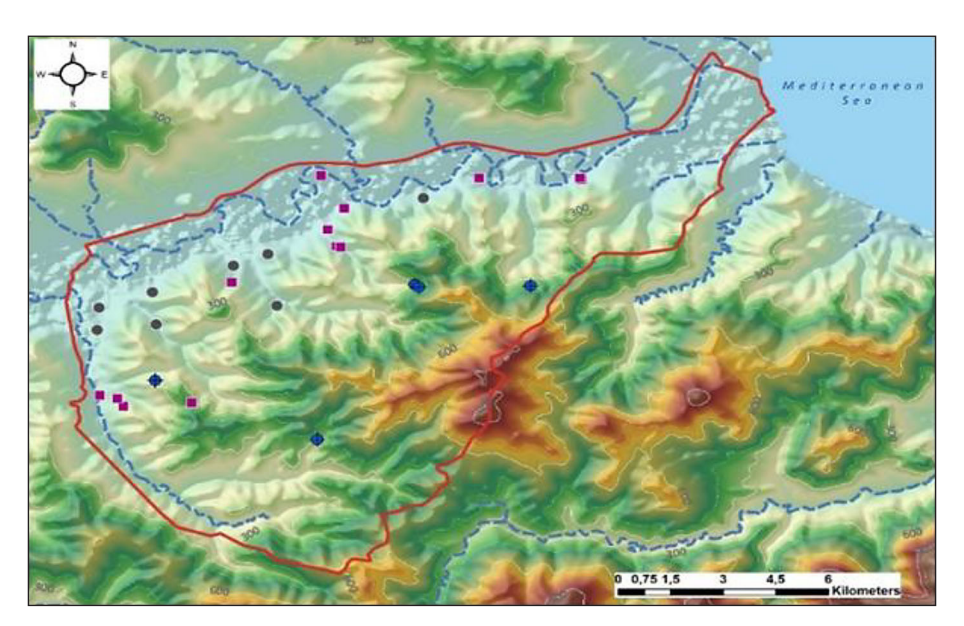


Figure 2. A topographic map of the Amizour's region

the Lower Cretaceous is observed in the study area and it is made up of marly limestone, black schist and beige limestone. Tertiary formations composed of the lower Eocene Marine, Marine Oligocene, and lower Marine Miocene. The Miocene is represented by sedimentary rocks on the left side of Soummam river, these rocks contain marl-sandstone alternation, conglomerates, fine and coarse sandstones (Hassissène, 1989), while, the igneous rocks which include Tonalite, Granitoid, Monzodiorite, Quartz monzonite,

Granite, Andesite, Rhyolite and Andesitic tuffs (Semroud,1981) are located in the Amizour region on the right side of the river. The Miocene formations with high fracturing level enhance the water circulation and favors aquifer's constitution. Marly shale, Coarse and quartz Sandstones form the Oligocene. Quaternary formations located alongside the Soummam River and its tributaries, Sand, gravel, and cobbles are its main constituents and they are characterized by their high – capacity of retention subterranean

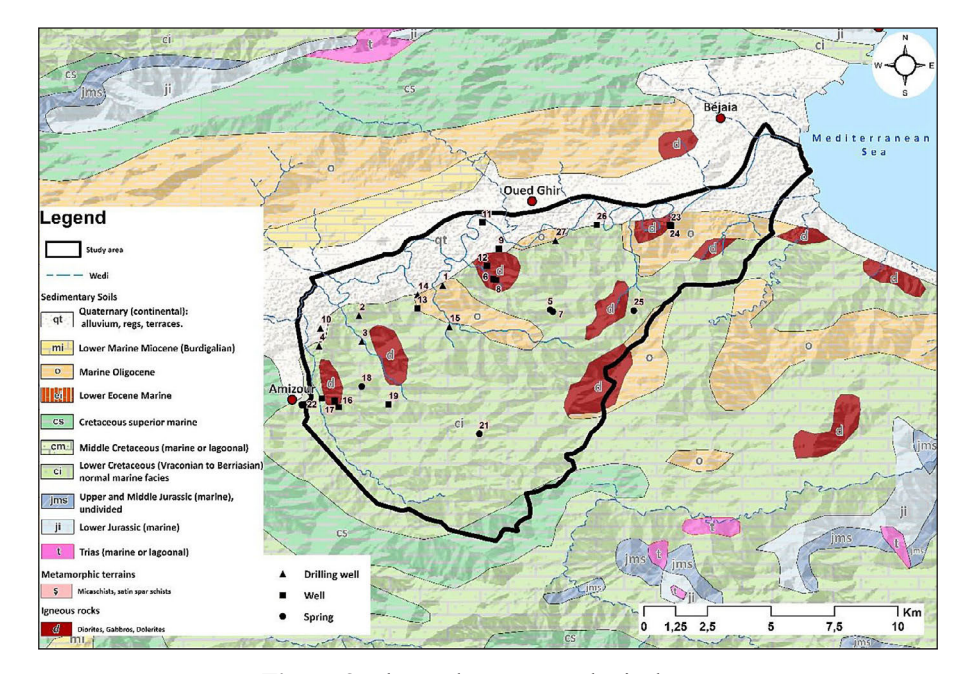


Figure 3. The study area's geological map

The General Company of Geophysics (CGG, 1970) completed by mechanical drilling in the alluvial plain shows the presence of two formations that constitute the Mio-Plio-Quaternary aquifer of lower Soummam, a discontinuous clayey layer separates these two units, indicating hydraulic connectivity between them. According to Clinckx (1973), this aquiclude is characterized by silty clay from Oued Amizour to Bejaia, indicating a semiconfined aquifer, while it is dominated by sandy clay upstream of the study zone, signifying a unconfined aquifer. The groundwater flow is from western to eastern. Figure 4 shows the several mineral deposits of the previously discussed region.

Sampling and field measurements

The groundwater sampling protocol was designed in accordance with ISO 5667-1 (ISO, 2020) and ISO 5667-11 (ISO, 2009) standards in order to collect twenty-six (26) samples and two (02) samples as duplicates from the study area during the high and the low water period. Prior to sampling, the purging operation was carried out at least three times. The calculated purge volume and the temperature, TDS, EC, and pH were measured for each purge volume. The samples were collected when the temperature, conductivity, and pH changes between the last two sets of field measurements

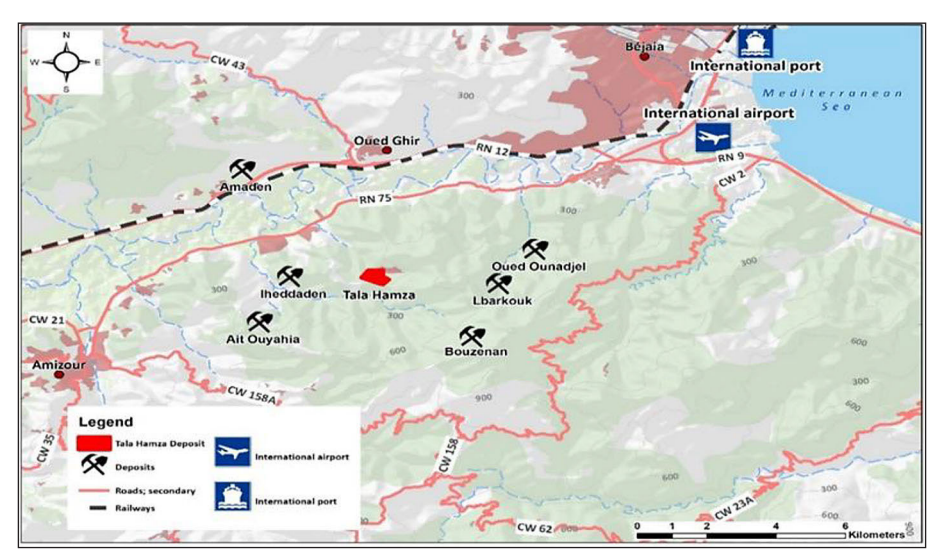


Figure 4. Map illustrating the mineral deposits in the research area

within the following ranges: ± 0.2 °C, ± 0.3 %, and ± 0.1 units, respectively. A hand-held GPS was used to record the samples' locations. The physical parameters including (T°, EC, TDS and pH) were measured on site using a certified thermometer (HANNA checktemp), a multi-parameter (HAN-NA HI 99300) (Figure 5a), and a pH-meter (Ohaus starter 300). One hundred milliliters (100 ml) of water were collected from each sampling points in acid-washed plastic bottles, The water was filtered using 0.45 µm membrane filter (Figure 5b), and then acidified with nitric acid (HNO₂) to a pH of 1-2 (Figure 5c), for the identification of trace elements. For the major ions, an additional 1L samples was taken from each sampling locations. Preservation and handling procedure of water samples were conducted according to ISO 5667-3 (ISO, 2018). During transportation, samples were stored in a cooling device that could keep the temperature at 5 \pm 3 °C, as well as all laboratory test were conducted respecting the samples maximum storage time.

Laboratory analysis

A complex-metric titration with a 0.05 mol/l ethylene diamine tetra acetic acid (EDTA) solution was utilized for calcium (Ca⁺²) and magnesium (Mg⁺²) analysis. Sodium (Na⁺) and potassium (K⁺) concentrations were measured using the Flame-Photometer (Model S-931). Ion chromatography (Dionex ICS 3000 Model) was used to identify the chloride (Cl⁻) and bicarbonate (HCO₃), while nitrate (NO₃⁻) and sulfate (SO₄⁻²) were determined through UV visible

spectrophotometer (DR 5000). Traces elements (Zn, Pb, Fe, Mn, Li, Ni, Cd and Co) were quantified by Graphite furnace atomic absorption spectroscopy (GFAAS), Analytik Jena-contrAA 800 Model. Prior to samples analysis, calibration was performed using standards solutions (Figure 6) to ensure the accuracy and the reliability of the measurements.

The calibration curve is always represented graphically by plotting absorbance values of the standard solutions on the vertical (Y) against their known concentrations on the horizontal axis (X), In the present study calibration curve were prepared using a series of standards concentrations ranging from 0 to 1 mg/l (0, 0.25, 0.5, 0.75 and 1 mg/l) for Zn, Pb, Mn, Li, Cd and Co, and from 0 to 2 mg/l (0, 0.5, 1, 1.5 and 2 mg/l) for Fe and Ni (Figure 7). The linear regression equation obtained from calibration curve was adopted to calculate the concentration of analytes. Figure 8 represents the results showing the maximum concentrations of Fe and Mn detected in sample n° 06.

The relative percent difference Equation 1 was calculated to quantify duplicate results. For aqueous samples, an RPD of $\leq 20\%$ may often considered an acceptable result.

$$RPD = \frac{(C1 - C2)}{[C1 + C2)/2]} \times 100 \tag{1}$$

where: C1 – concentration of analyte in sample 1 and C2 – concentration of analyte in sample 2.

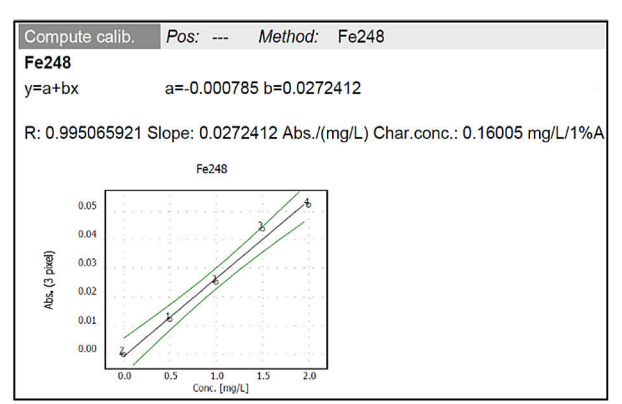
The charge balance error Equation 2 within $\pm 5\%$ indicates that the analytical result is acceptable.



Figure 5. (a) Multiparameter HANNA HI 99300 for TDS and EC in filed measurement, (b) in field sample's filtration using 0.45 μm membrane filter, (c) sample acidification to pH of 1–2 by HNO₃



Figure 6. Atomic absorption spectroscopy-standards solutions for curve calibration



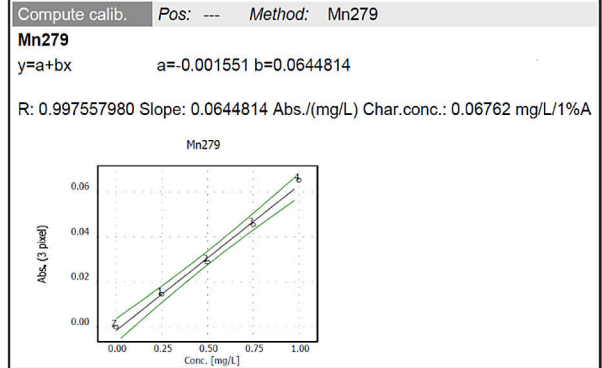


Figure 7. The calibration curve with linear regression equations of iron and manganese

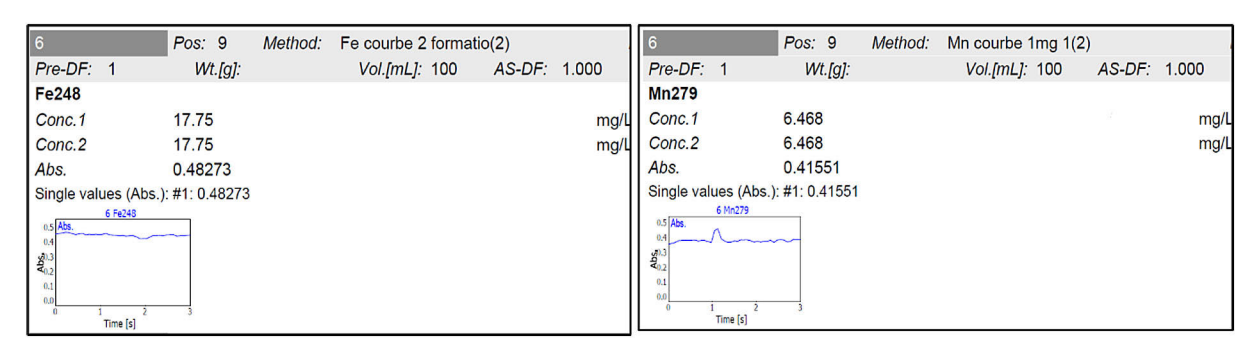


Figure 8. The data output from AAS, showing absorbance and higher concentrations of Fe and Mn during the low-water period

$$CBE = \frac{\sum \text{Cations}\left(\frac{\text{meq}}{1}\right) - \sum \text{Anions}\left(\frac{\text{meq}}{1}\right)}{\sum \text{Cations}\left(\frac{\text{meq}}{1}\right) + \sum \text{Anions}\left(\frac{\text{meq}}{1}\right)} \times 100 \quad (2)$$

All of the samples RPD and CBE in this study meet the standards, indicating that the results are reasonable and sufficient.

Statistical analysis

Data were statistically analyzed using a combination of descriptive, bivariate and multivariate statistical techniques to identify patterns and relationships among the measured groundwater quality parameters. All statistical analyses were performed using Microsoft Excel integrated with the XLSTAT software package.

GIS analysis

In this study ESRI ArcGIS software (v 10.8) was used and Kriging method was employed to perform spatial interpolation. Both physicochemical parameters and spatial information obtained from field sampling and laboratory analysis were compiled into a single Excel spreadsheet. To guarantee spatial compatibility, each sampling

point was assigned exact geographic coordinates in latitude and longitude, which projected to WGS 1984 UTM Zone 31N coordinate system (Figure 9). Each parameter was imported into ArcGIS and linked to the georeferenced sampling point for processing to generates spatial distribution maps using kriging interpolation technique. Ordinary kriging, used in the present study (Figure 10), generates the most effective prediction in groundwater distribution compared to other kriging techniques (simple and universal), showing lower root mean squared error (RMSE) values and less points with significant deviation between

estimated and predicted values (Yao, 2014). The spherical semi variogram model was used for representing spatial variability. Figure 11 illustrates the pH interpolation results in the study area during the low-water period.

The Geostatistical Analyst module of Arc-GIS 10.8's Cross Validation tool was utilized to evaluates and assess the performance and reliability of the variogram model. The results (Figure 12) of pH interpolation, show a mean error (ME) close to zero (0.014), indicating no significant bias between predicted and measured values. Furthermore, the RMSSE value of 0.905, being

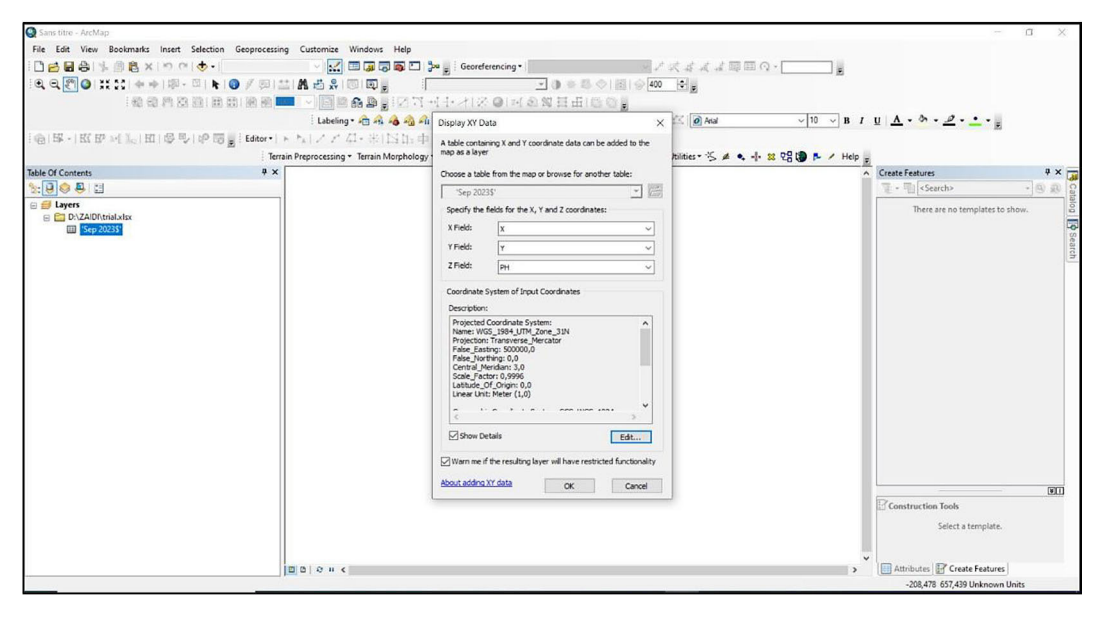


Figure 9. Screenshot illustrating ArcGIS data import interface

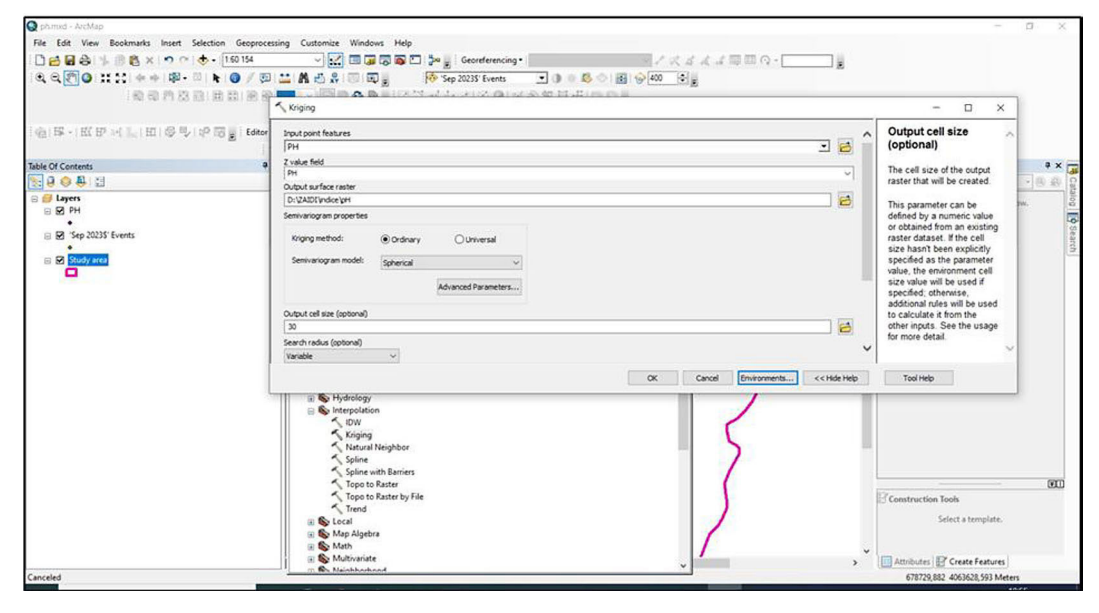


Figure 10. Screenshot from ArcGIS illustrating the selection of the kriging interpolation type and the semi variogram model

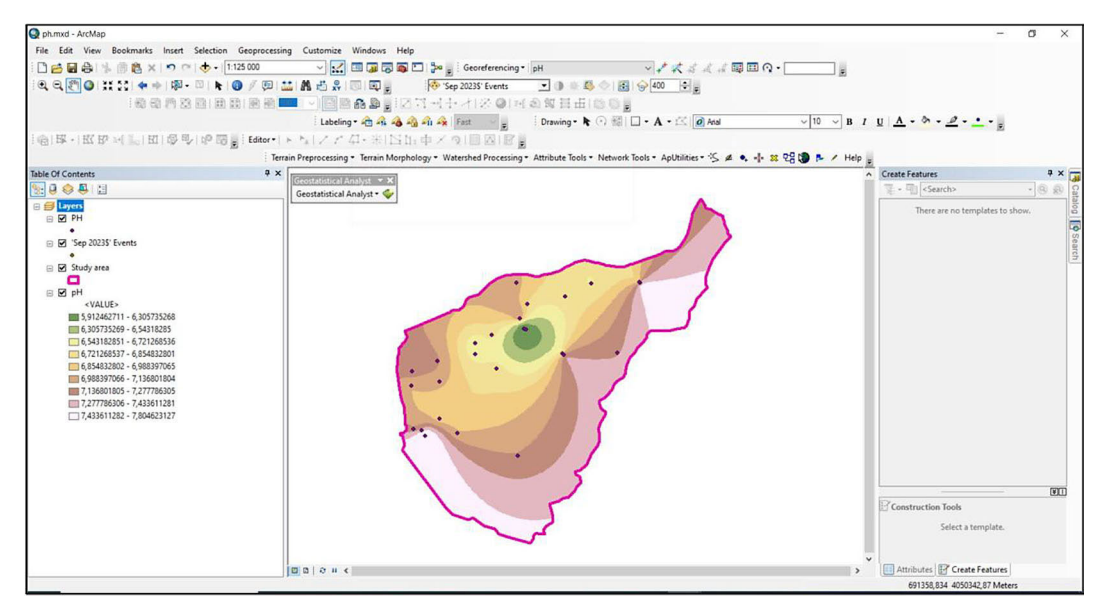


Figure 11. Screenshot showing kriging results of pH during the low-water period

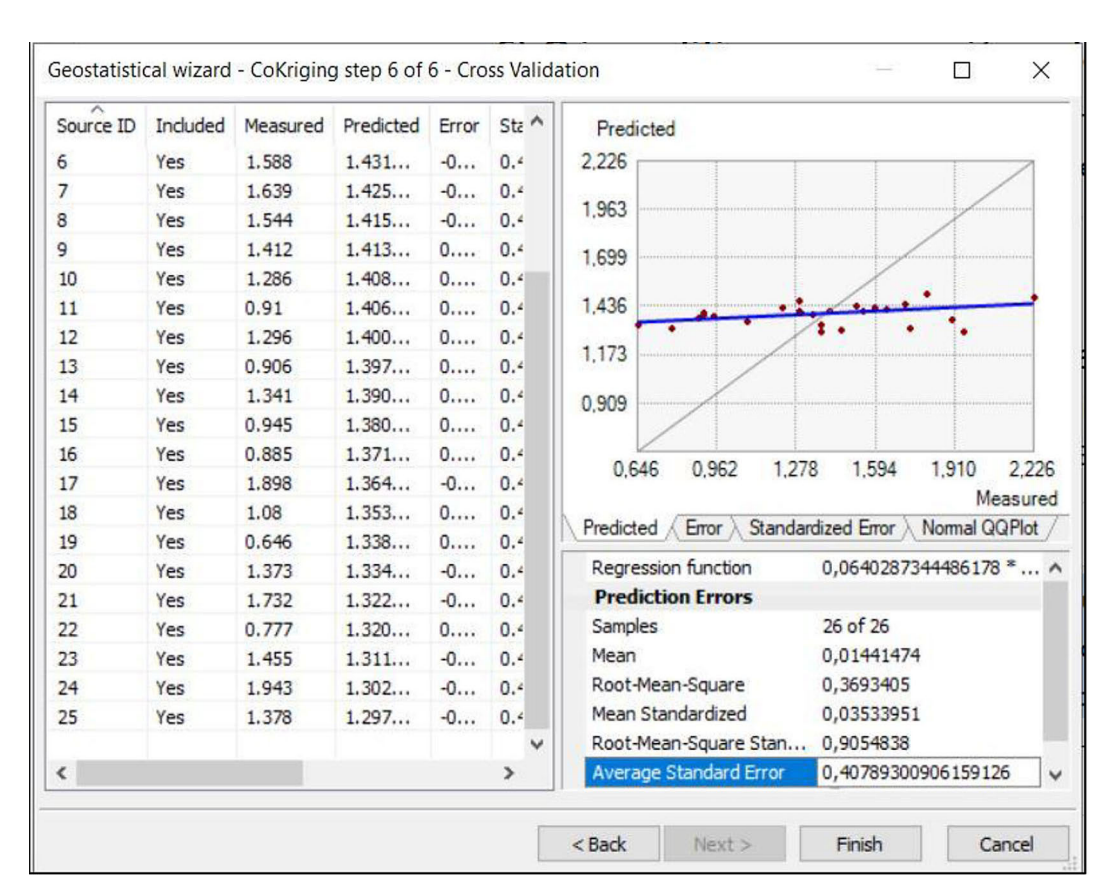


Figure 12. Cross-validation results for the kriging model applied to pH including scatter plot of predicted vs measured values and statistical summary of performance indicators (ME, RMS, ASE, RMSSE) generated using the Geostatistical Analyst tool in ArcGIS 10.8

close to 1, confirms the consistency and reliability of the variogram model used for the interpolation groundwater's pH within the study area during the low-water period. Based on the best validated variogram through cross-validation, the

prediction maps for the spatial distribution of various groundwater quality parameters were generated (Balaji, 2025).

Stretched symbology with the histogram equalize option, was used for presenting the final

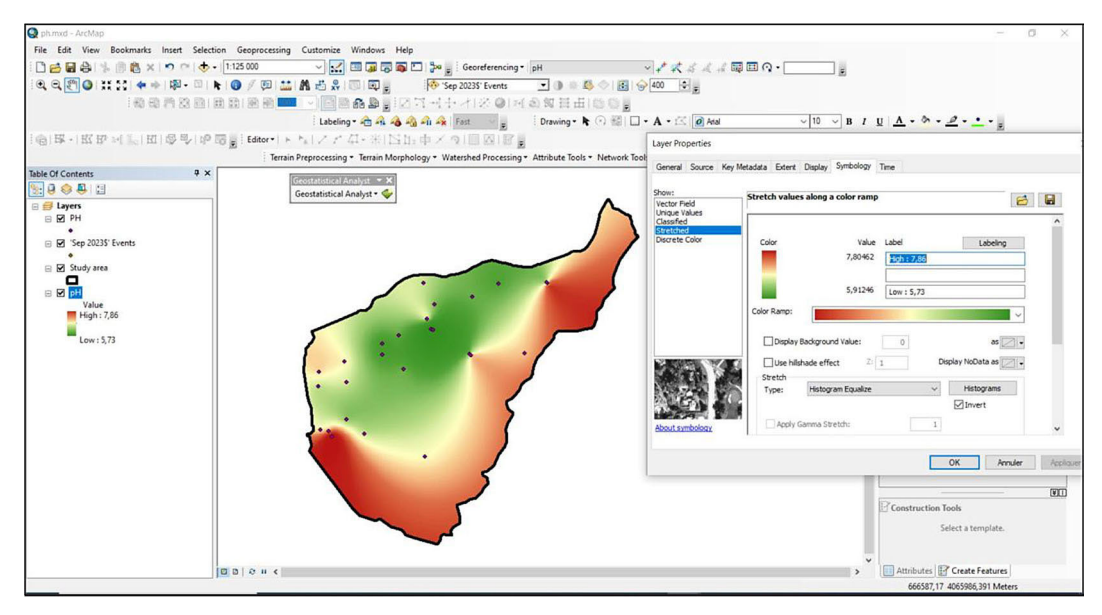


Figure 13. Screenshot sowing the stretched symbology for final map visualization

map (Figure 13), in order to enhance visual contrast, as well as, facilitate the reading of spatial concentration gradients.

RESULTS AND DISCUSSION

Descriptive data and spatiotemporal distribution

All measured physical parameters and chemical elements from samples collected during both water periods were summarized using descriptive statistics (Table 1), including the minimum, maximum, mean and standard deviation for each variable. The percentage of samples exceeding detection limits was calculated to assess the distribution and mobilization of elements within the study area. Notably, during the high-water period, a higher percentage of samples showed values above the detection limits compared to the low-water period, this suggests that precipitation is causing a significant weathering, diffusion and dilution of metals, specifically Zn, Pb, Fe, Cd, Mn, and Ni.

Electrical conductivity (EC) averaged $1450.08 \pm 537;77~\mu S/cm$ in the low-water period and $1091.7 \pm 504.76~\mu S/cm$ in the high-water period, indicating that the low-water conditions favor mineral concentrations due to the reduced recharge, whereas high-water conditions encourage diffusion and dilution of dissolved ions (Figure 14). The pH ranged from 5.73 to 7.86, with an average of 6.94 during the low-water period (September), and in the high-water period (March),

it varied from 6.70 to 7.77, averaging 7.18. In both periods groundwater's nature almost neutral, except one sample in the low water period, with acidic character referring to manganese' and iron's highest values, this sample is located in the middle of the study area near to Tala Hamza deposit (Figure 15).

Under natural conditions, the geochemical content of groundwater is regulated by the primary cations Ca²⁺, Mg²⁺, Na⁺, and K⁺, along with the primary anions HCO₃-, SO₄²-, and Cl-In contrast, NO₃ is more frequently a consequence of human activities on the surface (Saha et al., 2023). The anions concentrations were in the order HCO₃⁻ > SO₄²- > Cl⁻ > NO₃⁻ during the low-water period and HCO₃ > Cl > SO₄2- > NO₃ during the highwater period. In contrast, cations concentrations followed a consistent sequence of Ca2+ > Na+ > $Mg^{2+} > K^+$ in both periods. The dominance of HCO₃ among anions and Ca²⁺ among cations during both periods, indicates that carbonates or/and silicates weathering is the primary process controlling the Soummam's groundwater chemistry. The secondary abondance of Na⁺ among cations and SO₄² during the low-water period, along with Cl during the high-water among highlight the contribution of Triassic evaporitic dissolution and marine intrusion to groundwater hydrochemistry, which is consistent with earlier finding reported by Saou et al. (2012), Ouyahia et al. (2024) and Kessasra et al. (2021).

During the high-water period, major ions generally decreased in parallel with the reduction in

Table 1. 1	Descriptiv	ve statisti	cal data o	f groundy	vater sam	ples in th	e study ar	ea					
\/orioblo	1.1		Septer	mber 2023	(n=26)		March 2024 (n=22)						
Variable	Unit	Min	Max	Ave	Std dev	%>dl	Min	Max	Ave	Std dev	%>dl		
Τ°	C°	18.40	22.90	20.82	1.10	100%	13.40	21.40	17.57	2.23	100%		
рН	pH unit	5.73	7.86	6.94	0.43	100%	6.70	7.77	7.18	0.26	100%		
TDS	mg/l	289.00	1495.00	750.42	277.54	100%	141.00	883.00	547.05	240.53	100%		
EC	μS/cm	556.00	2874.00	1450.08	537.77	100%	237.00	1989.0	1091.7	504.76	100%		
Ca ²⁺	mg/l	44.09	364.71	157.85	69.74	100%	15.79	216.00	113.44	62.27	100%		
Mg ²⁺	mg/l	12.15	98.44	39.03	19.11	100%	4.80	62.40	23.47	16.22	100%		
Na⁺	mg/l	27.00	184.00	71.03	43.67	100%	14.17	141.67	65.60	36.96	100%		
K+	mg/l	2.00	16.00	6.74	4.28	100%	3.00	22.00	8.95	5.15	100%		
NO ₃ -	mg/l	4.61	48.90	17.19	10.85	100%	2.84	63.57	16.00	14.55	100%		
HCO ₃ -	mg/l	176.95	497.29	335.83	107.91	100%	46.97	390.40	222.89	105.76	100%		
CI-	mg/l	55.80	395.00	150.35	83.34	100%	44.99	346.39	141.41	80.23	100%		
SO ₄ ² -	mg/l	39.44	421.99	173.09	103.20	100%	16.00	200.00	114.53	63.74	100%		
Zn	mg/l	<dl< td=""><td>4.747</td><td>0.537</td><td>1.034</td><td>81%</td><td><dl< td=""><td>3.069</td><td>0.550</td><td>0.880</td><td>91%</td></dl<></td></dl<>	4.747	0.537	1.034	81%	<dl< td=""><td>3.069</td><td>0.550</td><td>0.880</td><td>91%</td></dl<>	3.069	0.550	0.880	91%		
Pb	mg/l	<dl< td=""><td>0.207</td><td>0.038</td><td>0.064</td><td>38%</td><td><dl< td=""><td>6.990</td><td>0.641</td><td>1.582</td><td>50%</td></dl<></td></dl<>	0.207	0.038	0.064	38%	<dl< td=""><td>6.990</td><td>0.641</td><td>1.582</td><td>50%</td></dl<>	6.990	0.641	1.582	50%		
Fe	mg/l	<dl< td=""><td>17.750</td><td>0.929</td><td>3.585</td><td>15%</td><td><dl< td=""><td>1.440</td><td>0.324</td><td>0.454</td><td>95%</td></dl<></td></dl<>	17.750	0.929	3.585	15%	<dl< td=""><td>1.440</td><td>0.324</td><td>0.454</td><td>95%</td></dl<>	1.440	0.324	0.454	95%		
Li	mg/l	0.004	0.134	0.042	0.034	100%	0.009	0.098	0.026	0.019	100%		
Co	mg/l	0.012	0.039	0.021	0.006	100%	0.007	0.055	0.024	0.013	100%		
Mn	mg/l	<dl< td=""><td>6.468</td><td>0.655</td><td>1.335</td><td>69%</td><td>0.015</td><td>4.137</td><td>0.260</td><td>0.876</td><td>100%</td></dl<>	6.468	0.655	1.335	69%	0.015	4.137	0.260	0.876	100%		
Cd	mg/l	<dl< td=""><td><dl< td=""><td><dl< td=""><td>-</td><td>0%</td><td><dl< td=""><td>0.043</td><td>0.003</td><td>0.010</td><td>18%</td></dl<></td></dl<></td></dl<></td></dl<>	<dl< td=""><td><dl< td=""><td>-</td><td>0%</td><td><dl< td=""><td>0.043</td><td>0.003</td><td>0.010</td><td>18%</td></dl<></td></dl<></td></dl<>	<dl< td=""><td>-</td><td>0%</td><td><dl< td=""><td>0.043</td><td>0.003</td><td>0.010</td><td>18%</td></dl<></td></dl<>	-	0%	<dl< td=""><td>0.043</td><td>0.003</td><td>0.010</td><td>18%</td></dl<>	0.043	0.003	0.010	18%		
Ni	ma/l	-dl	~dl	-dl	_	0%	~dl	0.188	0.012	0.041	14%		

Table 1. Descriptive statistical data of groundwater samples in the study area

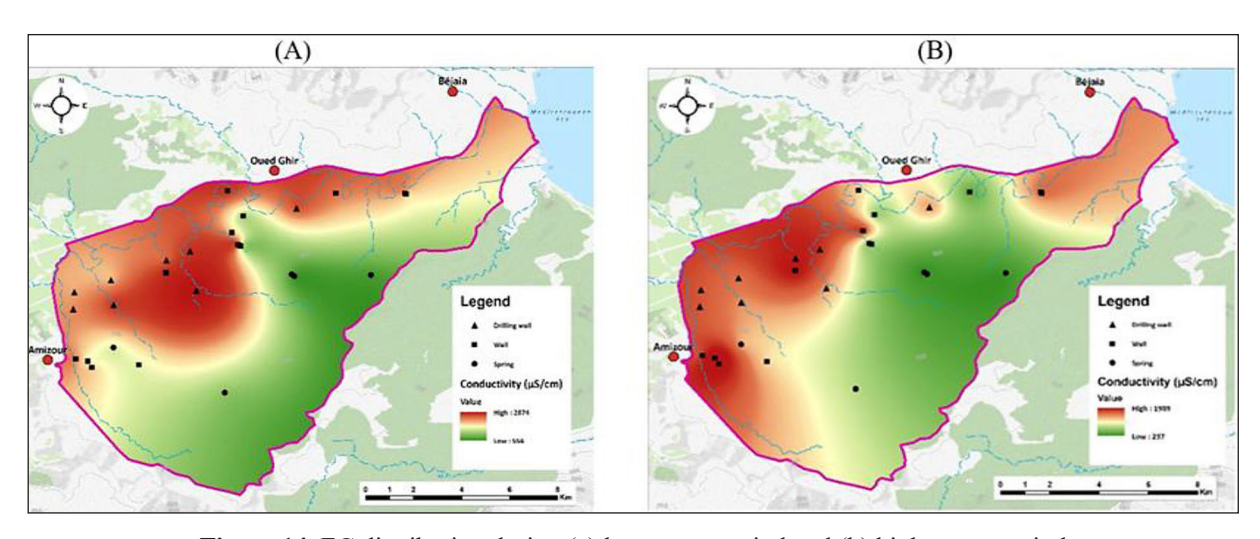


Figure 14. EC distribution during (a) low-water period and (b) high-water period

total dissolved solids (TDS) and electrical conductivity (EC) compared to the low water period. However, Potassium (K+) exhibited an opposite trend, increasing from 6.74 mg/l to 8.95 mg/l, suggests additional inputs that's possibly associated with human activities or agricultural runoff.

Lithium concentrations decreased from an average of 0.042 mg/l during the low-water period to 0.026 mg/l during the high-water period

(Figure 16), confirming the influence of recharge and seasonal hydrodynamics, and aligning with Jalali (2009), reported that in rock water interaction, elevated temperature enhance Lithium enrichment. During the low-water period, Cobalt reached 0.039 mg/l (Figure 17), in the same low-pH samples, co-occurring with elevated Fe, Mn and Li concentrations near the Tala Hamza deposit, which localized within igneous rocks and

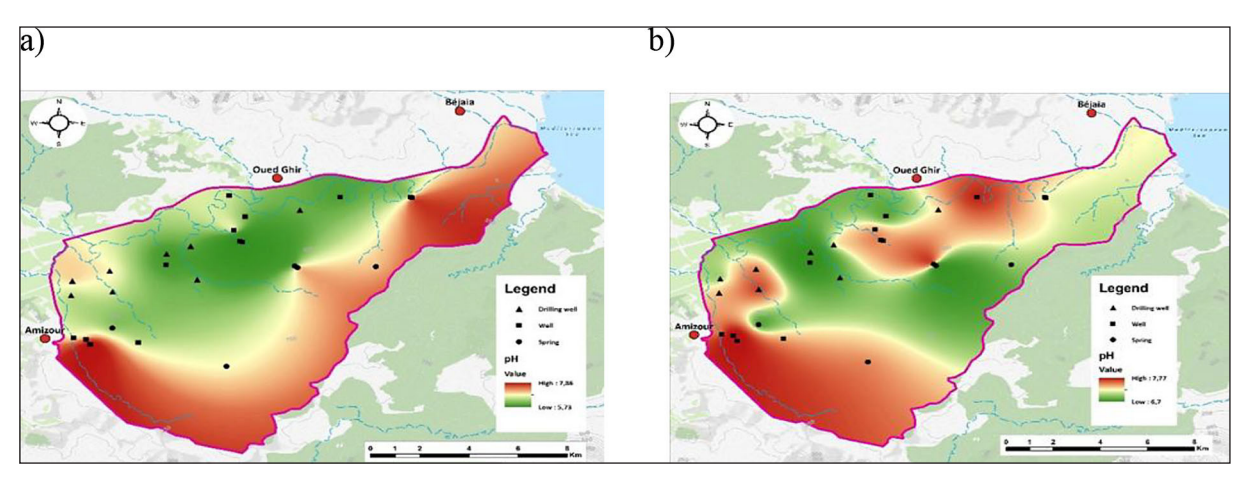


Figure 15. pH distribution during (a) low-water period and (b) high-water period

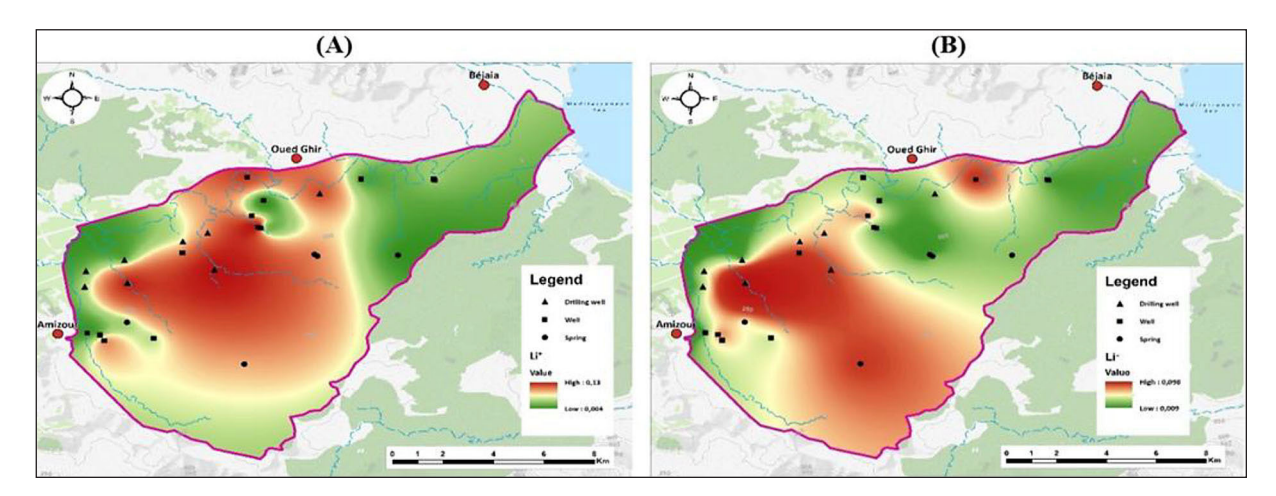


Figure 16. Spatio-temporal distribution of lithium during (a) low-water period and (b) high-water period

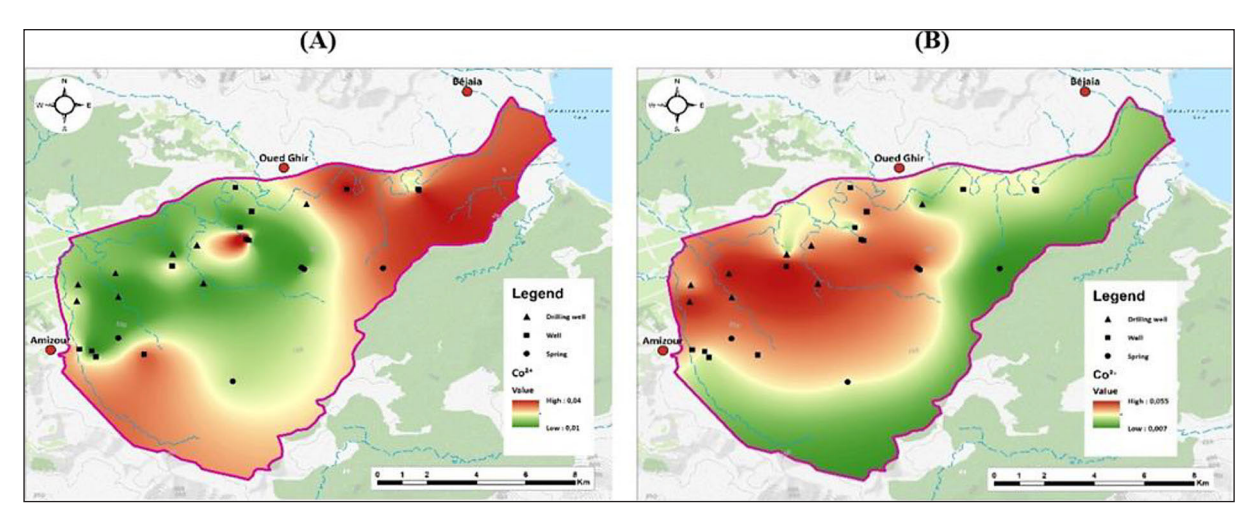


Figure 17. Spatio-temporal distribution of Cobalt during (a) low-water period and (b) high-water period

Marine Oligocene strata, suggesting theses lithologies as a potential source of metals.

During the low-water period, most samples exhibiting elevated Zn concentrations were located

within agricultural area, which could be related, according to Raza (2023), to Zn-enriched fertilizers use. The other samples are concentrated in the southwest of the region between Amizour's river

and Ait Ouyahia deposit which could be its origin. In contrast, in high-water period sampling points are clustered downstream of the study area from Ait Ouyahia deposit to the eastern side in the same direction of groundwater's flow (Figure 18). Lead concentrations averaged 0.038±0.064 mg/l during the low-water period and increased to 0.64±1.582 mg/l during the high-water period (Figure 19), highlighting a significant seasonal variation and an important spatial heterogeneity in Pb distribution.

Iron in groundwater originates primarily from natural source. According to previous research, pyrite oxidation is another important geochemical process that mobilizes iron in groundwater. Davidson (1993) noted that Fe and Mn naturally coexist in groundwater because of similarities in chemical properties. Likewise, in the present study, acidic pH conditions appear to enhance iron (Fe) and manganese (Mn) solubility during the low-water period, with the highest Fe and Mn concentrations

coinciding with the lowest pH values in a sample collected near to Tala Hamza deposit. During the low-water period, iron distribution was localized, with detectable concentrations occurring in only 15% of the samples collected in proximity to Tala Hamza area (Figure 20A). On the other hand, iron was identified in 95% of samples during the highwater period (Figure 20B), indicating elevated concentrations downstream of Tala Hamza, which suggests iron mobilization and transport under recharge conditions. The Manganese exceed the detection limits in all samples (Figure 21) in both periods highlighting their geological origin.

As stated by Abraham et al. (2024), cadmium has been identified as the heavy metal that poses the highest concern to the environment because of its harmful impacts. In the present study, Cadmium exhibited a trend similar to that of Nickel (Figure 22). Their concentrations exceed the detection limits in only 18% and 14% of the

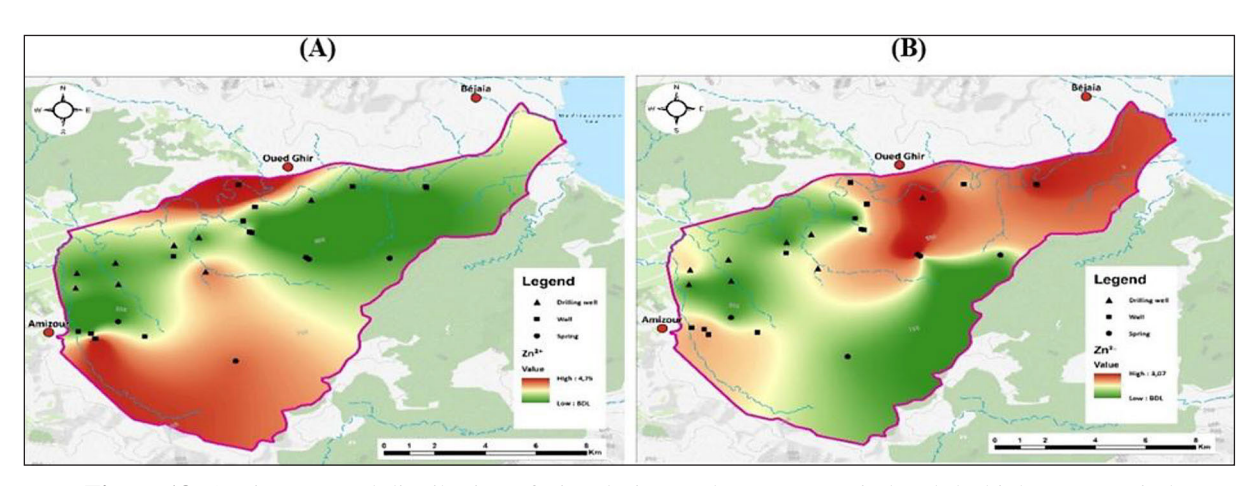


Figure 18. Spatio-temporal distribution of Zinc during (a) low-water period and (b) high-water period

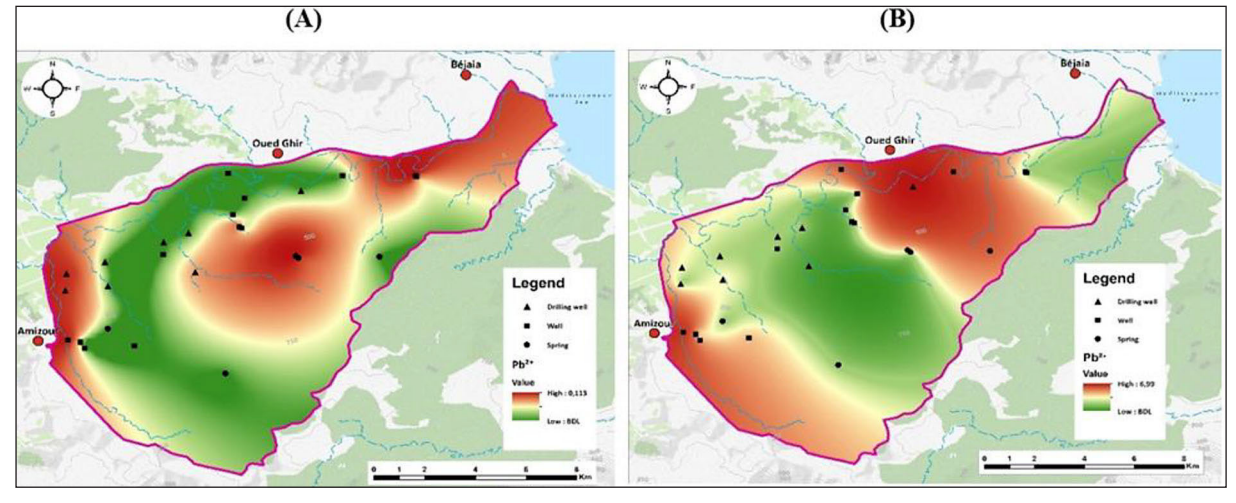


Figure 19. Spatio-temporal distribution of lead during (a) low-water period and (b) high-water period

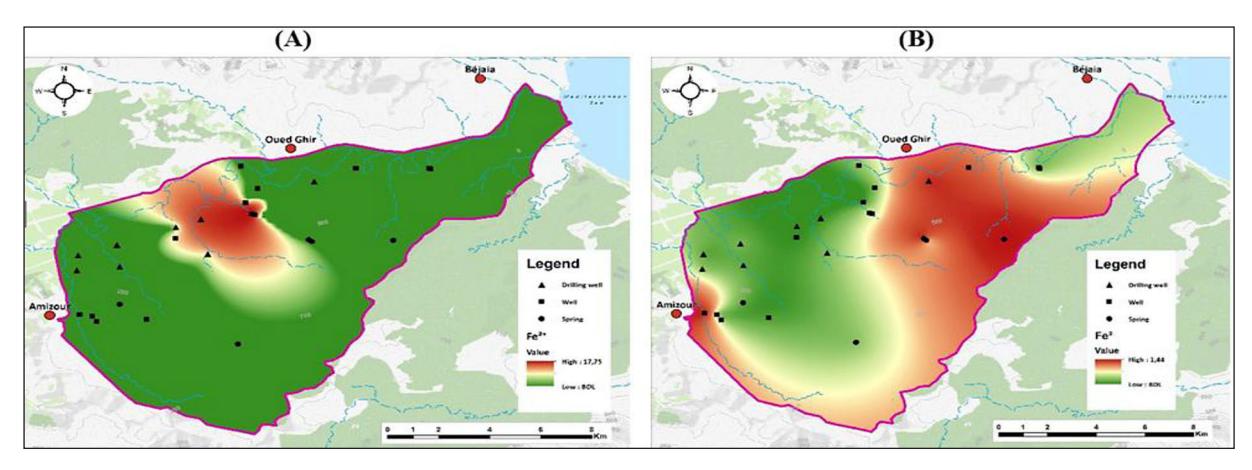


Figure 20. Spatio-temporal distribution of Iron during (a) low-water period and (b) high-water period

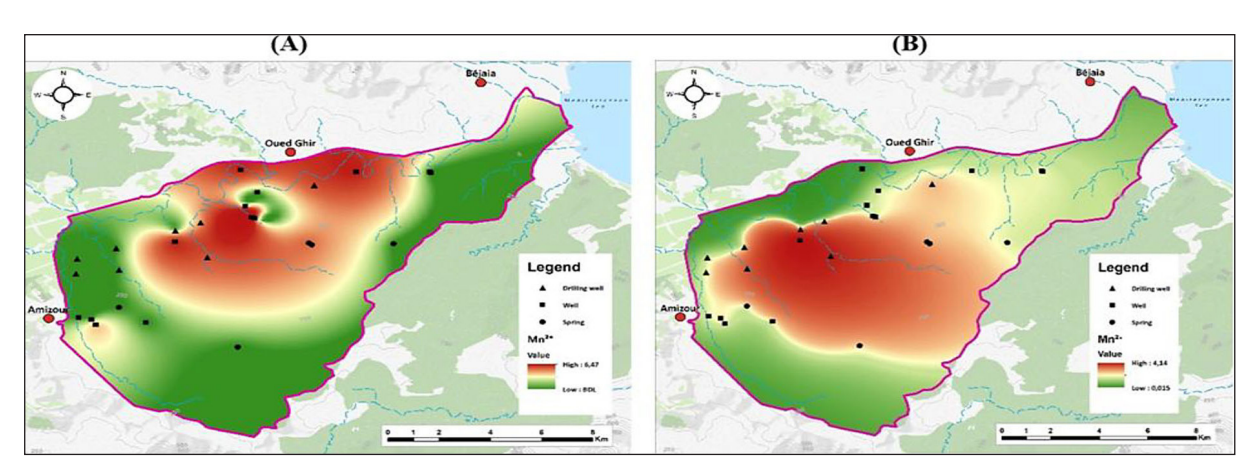


Figure 21. Spatio-temporal distribution of Manganese during (a) low-water period and (b) high-water period

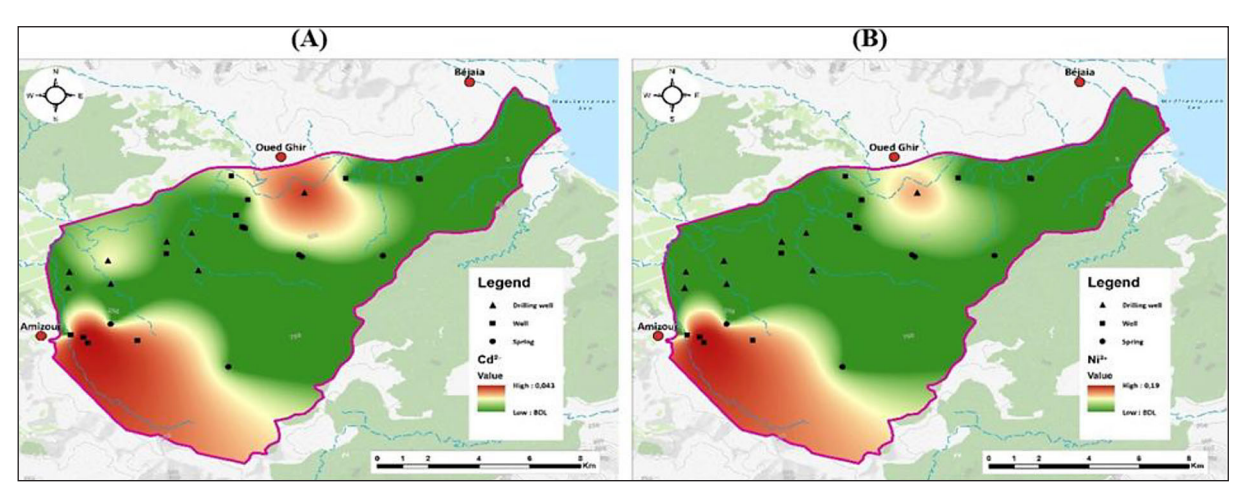


Figure 22. Spatial distribution of cadmium (A) and nickel (B) during high-water period

samples, respectively, during the high-water period, whereas, both metals were below detection limits during the low-water period. The highest concentrations of Cadmium and Nickel coincided with maximum nitrate levels (63.57 mg/l) near the Amizour river, suggesting a potential anthropogenic source for these metals' enrichment.

Factors controlling groundwater quality

The Gibbs diagram shown in Figure 23 illustrates the mechanism of natural evolution of the groundwater chemical component. The rock dominance is the essential process influencing the groundwater chemistry in both water periods.

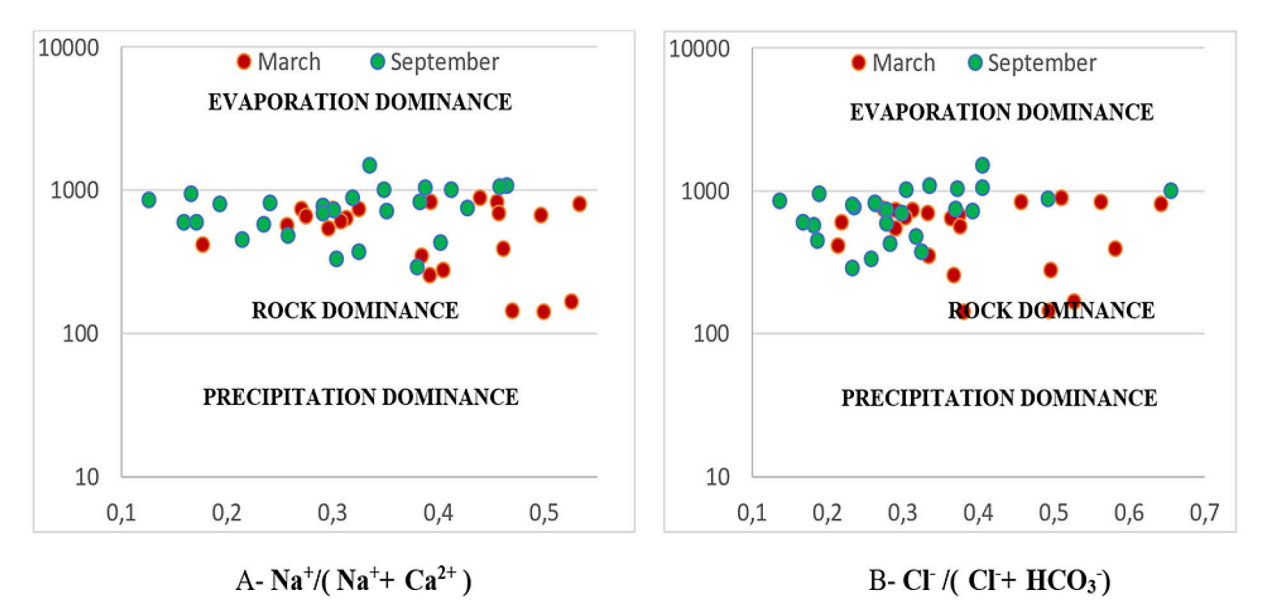


Figure 23. Gibb's plot showing major processes controlling groundwater chemistry

Evaporation domain is found only during the low water period, whereas, the precipitation process does not occur in the aquifer.

According to the Ca²⁺/Na⁺-HCO₃-/Na⁺ and Ca²⁺/Na⁺-Mg²⁺/Na⁺ diagrams (Figure 24), silicate weathering is the main geochemical process affecting groundwater quality in the study area. Considering the geological context, silicate minerals could be pyroxenes, plagioclase, biotite and feldspars, which are found in plutonic and volcanic rocks, and also could be from Sandstone occurred in the region. To understand the influence of silicate weathering, The sodium concentrations are plotted against the chloride concentrations (Figure 25). Most of groundwater samples lie below the 1:1 line, indicating excess of chloride compared to sodium.

The Na/Cl ratio falls to less than one, indicates that the sodium has been released from the

groundwater, as a result of silicate weathering and reverse ion exchange, which is identified as a major hydrogeochemical process governing the groundwater chemistry as shown by Chadha diagram (Figure 26).

Multivariate analysis of groundwater

The main purposes of multivariate statistical analysis of groundwater are to determine the variables influencing its quality and identify pollution sources. It serves to reduce the volume of data by grouping water samples with similar properties and finding correlations between water quality and its geological or anthropogenic environment. In this study, principal component analysis (PCA) and correlation matrix analysis were used to comprehend the relationship within groundwater quality data and analyze multiple parameters

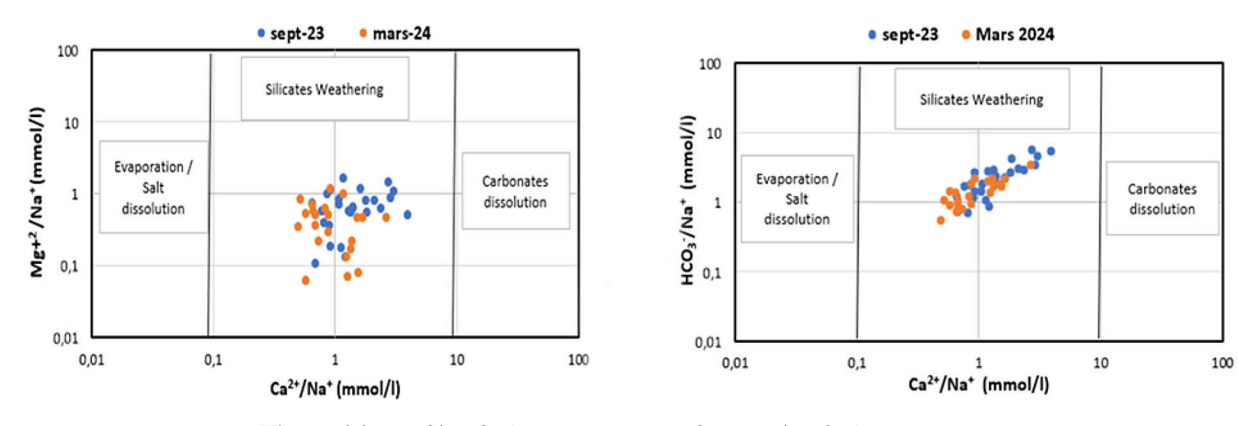


Figure 24. Mg+2/Ca+2 plot versus Na+ and HCO3-/Ca+2 plot versus Na+

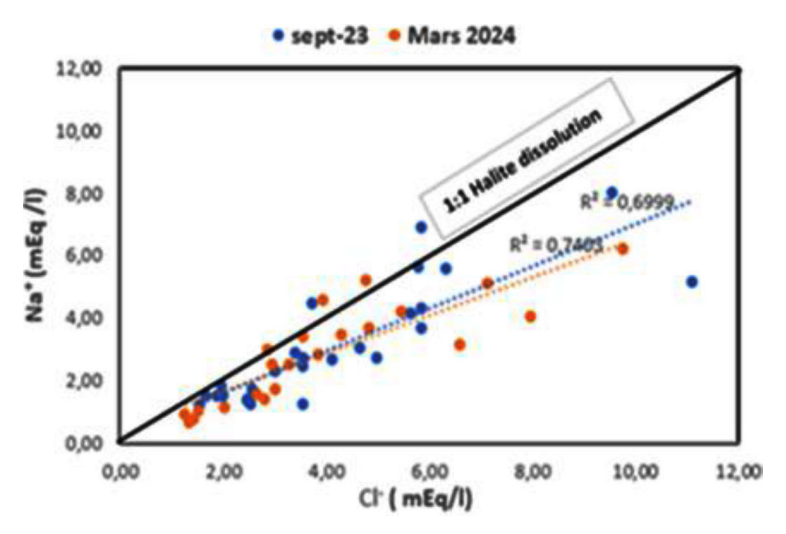


Figure 25. Na⁺/Cl⁻ ratio

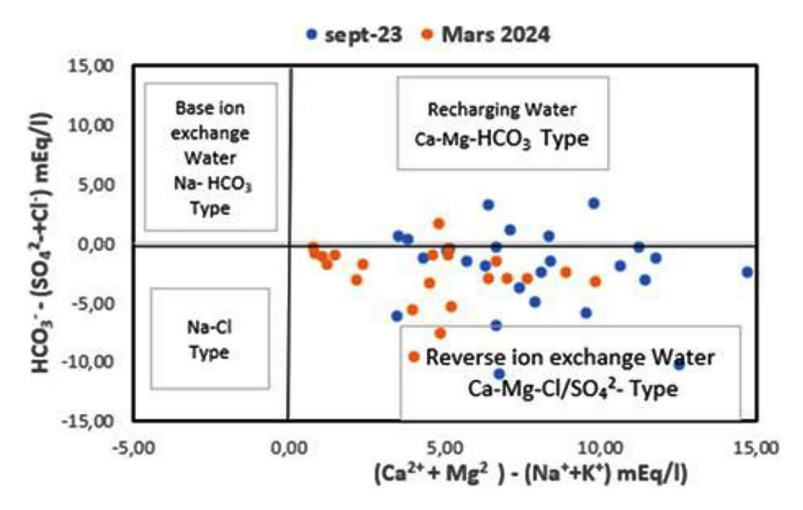


Figure 26. Chadha diagram of groundwaters samples

simultaneously. Although the PCA (Table 2) reduce all measured physicochemical parameters into a smaller sets of independents components, the Pearson correlation coefficient (Table 3) measure of the linear correlation between two variables.

Five components with eigenvalues≥1 were identified from the chemical variables data set using principal component analysis (Table 2) Their cumulative percentage is 74,47% in low- water period and 76,35% in high-water period.

The first factor represents 36.8% of the total variance, was primarily composed of TDS, EC, Na⁺, K⁺, SO₄⁻², lithium, Cl⁻ and Ca⁺² during lowwater period, while it shows 32.98% of the total variance, represented by EC, TDS, Ca⁺², Na⁺, Cl⁻, HCO₃⁻, SO₄⁻², NO₃⁻ and lithium during high-water period. The change in influencing variables in both periods can be associated with variations in

patterns of rainfall, in addition, it might be related to water-rock interaction, dissolution of Gypsum and Halite as well as natural processes including silicate weathering, seawater intrusion, reverse ion exchanges. Chloride exhibits a strong correlation in both periods with Na⁺, indicating that the rock salt (halite) serves as their principal source. However, $SO_4^{\ 2^-}$ and Cl^- show a moderate correlation during the two periods of September (0.66) and March (0.69), whereas $SO_4^{\ 2^-}$ has a strong correlation with Ca^{+2} (r=0.86) during both periods, pointing to $SO_4^{\ 2^-}$ is mainly generated by evaporites dissolution (gypsum, anhydrites) of trias genesis.

Cadmium and nickel showed the strongest relationship (0.97) during the high-water period, as well as their correlation with NO₃⁻, suggests that agricultural practices are the source of these pollutants. The two elements (Cd and Ni) represent a significant loading on the second component (F2)

showing 17.25% of the total variance during the high-water period.

During the low-water period, the same component (F2) explains 15.51% of the total variance and describes the significant contributions of Mn (0.72), Fe (0.71), Co (0.68), Mg (0.49) and negatively with pH (-0.54). The Pearson matrix explores the very high positive correlation between Fe and Mn (0.87) in September period, as well as pH has a moderately negative correlation with these two variables, highlighting that an acidic environment stimulates the release of these metals, furthermore, they have a moderate correlation with Cobalt, in addition, a moderate correlation between Iron and Magnesium was observed. Considering these results of PCA and correlation matrix with the region's geological background and the spatial distribution of these elements near to Tala Hamza (Ait Bouzid) deposit, highlights the contribution of Oligocene quartzite-sandstone fragments enclosed in pyroclastic breccias and Silicate minerals of igneous rocks such pyroxenes and biotite in their presence in the groundwater.

The loading of HCO₃ on F3 (0.6) during the low-water period, and its correlation with both

Ca+2 and Na+ indicates its release into groundwater by the calcite dissolution from limestone of lower Cretaceous observed in the study area and by the dissolution of sodium-bearing silicate minerals. During the high-water period, the third component exhibit a moderate negative value for lead (-0.57) and zinc (-0.45) showing that these two elements have a negative contribution to this factor, in addition to the Pearson matrix that shows a moderate correlation (0.51) between these two elements, which are also moderately correlated with iron, emphasizing presence of common origin for these three metals (iron, zinc and lead). This source could be the natural leaching of these polymetallic elements from the local deposits, particularly Tala Hamza, which is occurs in the center of the study area. F3 accounts 8.62% and 9.79% of the total variance in low-water and high-water period respectively.

In September, F4 and F5 accounts 7.31% and 6.22% of the total variance respectively. However, the fourth component encompasses zinc (0.7) which indicates high concentration adjacent the Soummam River and also between the Amizour river and Ait Ouyahia deposit, implying that its

Table 2. Correlation between variables and factors from PCA

Variables		Low	– water pe	riod		High – water period							
variables	F1	F2	F3	F4	F5	F1	F2	F3	F4	F5			
Ph	-0.374	-0.543	0.210	0.341	0.098	-0.024	0.690	0.254	-0.030	0.110			
TDS	0.953	-0.243	0.133	-0.074	-0.063	0.926	-0.183	-0.178	-0.195	0.010			
EC	0.951	-0.245	0.136	-0.086	-0.062	0.980	0.106	-0.094	-0.020	0.011			
Ca ²⁺	0.740	-0.393	0.416	0.075	-0.191	0.868	0.245	0.094	-0.223	0.147			
Mg ²⁺	0.427	0.485	-0.082	-0.041	0.272	0.404	-0.048	-0.424	0.099	-0.521			
Na⁺	0.895	-0.192	-0.181	-0.121	0.062	0.861	-0.248	0.018	-0.173	-0.029			
K ⁺	0.861	-0.228	-0.237	-0.116	0.071	0.135	-0.210	-0.400	0.672	0.394			
NO ₃	-0.043	-0.530	-0.111	-0.440	0.095	0.626	0.445	0.024	0.414	-0.188			
HCO ₃ -	0.531	-0.152	0.601	0.219	-0.046	0.805	0.301	0.051	-0.203	0.009			
Cl ⁻	0.769	-0.308	-0.271	-0.267	0.020	0.841	-0.164	-0.018	0.107	-0.053			
SO ₄ ²⁻	0.836	-0.007	0.292	0.022	-0.105	0.802	0.111	-0.330	-0.324	-0.092			
Zn	0.374	-0.106	-0.138	0.698	0.098	-0.245	0.379	-0.452	-0.349	0.243			
Pb	-0.047	0.195	0.333	-0.235	0.653	-0.093	0.368	-0.573	-0.499	0.319			
Fe	0.528	0.711	-0.207	-0.172	0.106	-0.596	0.296	-0.290	-0.370	0.279			
Li	0.807	0.233	-0.155	0.241	0.214	0.359	-0.121	0.223	0.200	0.358			
Co	0.245	0.683	0.262	0.093	-0.335	0.145	-0.401	0.559	-0.228	0.422			
Cd						0.318	0.830	0.034	0.203	0.119			
Mn	0.610	0.715	-0.074	0.071	-0.003	0.294	-0.455	0.015	0.115	0.659			
Ni						0.329	0.808	0.134	0.339	0.070			
%Variance	36.808	15.509	8.616	7.313	6.222	32.980	17.249	9.790	8.764	7.567			
∑variance	36.808	52.317	60.933	68.246	74.468	32.980	50.229	60.019	68.783	76.350			

Compants	рН	EC	TDS	Ca ⁺²	Mg ²⁺	Na⁺	K ⁺	HCO ₃ -	CI ⁻	SO ₄ ² ·	NO ₃ -	Zn	Pb	Fe	Li	Co	Cd	Mn	Ni
рН	1.00	0.25	0.29	0.25	0.19	0.18	0.17	0.27	0.20	0.15	0.13	0.02	0.29	0.10	0.35	-0.22	0.51	-0.32	0.49
EC	-0.24	1.00	0.97	0.91	0.64	0.91	0.43	0.80	0.90	0.85	0.48	-0.19	0.00	-0.47	0.40	0.24	0.01	0.39	-0.01
TDS	-0.24	0.91	1.00	0.86	0.66	0.89	0.44	0.76	0.86	0.83	0.51	-0.17	0.03	-0.48	0.23	0.16	0.06	0.31	0.03
Ca+2	-0.09	0.89	0.89	1.00	0.49	0.70	0.34	0.85	0.70	0.86	0.46	-0.05	0.26	-0.22	0.40	0.14	0.12	0.25	0.07
Mg ²⁺	-0.11	0.09	0.08	-0.19	1.00	0.66	0.30	0.52	0.64	0.62	0.42	-0.10	-0.22	-0.48	0.11	-0.02	-0.15	0.03	-0.14
Na⁺	-0.23	0.88	0.88	0.67	0.01	1.00	0.48	0.65	0.96	0.72	0.43	-0.20	-0.15	-0.47	0.37	0.34	-0.16	0.45	-0.17
K⁺	-0.26	0.87	0.87	0.64	0.05	0.98	1.00	0.20	0.48	0.50	0.57	-0.12	-0.13	-0.24	0.11	-0.01	0.07	0.44	0.11
HCO ₃ -	0.52	0.24	0.24	0.37	-0.05	0.06	0.06	1.00	0.58	0.62	0.49	-0.23	-0.09	-0.36	0.37	0.22	-0.03	0.12	-0.01
Cl-	-0.27	0.85	0.84	0.65	0.19	0.88	0.84	-0.08	1.00	0.69	0.44	-0.26	-0.23	-0.53	0.40	0.38	-0.11	0.46	-0.09
SO ₄ ²-	-0.39	0.87	0.87	0.86	0.06	0.68	0.67	0.01	0.66	1.00	0.35	0.17	0.38	-0.19	0.24	0.06	0.03	0.36	-0.07
NO ₃	0.15	0.04	0.04	0.02	-0.11	0.04	0.04	0.27	0.12	-0.27	1.00	-0.14	-0.21	-0.39	0.06	-0.20	0.63	-0.13	0.70
Zn	0.10	0.36	0.36	0.31	0.03	0.38	0.40	0.10	0.31	0.28	-0.16	1.00	0.51	0.46	-0.32	-0.04	0.20	-0.06	0.08
Pb	-0.07	0.01	0.00	0.05	-0.05	0.03	0.08	0.00	-0.03	0.07	-0.07	-0.15	1.00	0.62	-0.12	-0.31	0.28	-0.09	0.08
Fe	-0.58	0.27	0.27	-0.01	0.51	0.22	0.30	-0.50	0.43	0.31	-0.12	0.03	0.07	1.00	-0.29	-0.25	-0.02	-0.16	-0.10
Li	-0.34	0.71	0.71	0.55	0.32	0.65	0.68	-0.14	0.69	0.73	-0.31	0.48	0.08	0.51	1.00	0.06	0.03	0.30	0.07
Co	-0.25	0.03	0.03	-0.04	0.18	-0.09	-0.03	-0.21	-0.01	0.15	-0.35	0.00	-0.01	0.60	0.05	1.00	-0.21	0.55	-0.20
Cd	-	-	-	-	-	-	-	-	-	-	-	-	-	-	-	-	1.00	-0.08	0.97
Mn	-0.59	0.38	0.39	0.17	0.33	0.29	0.36	-0.41	0.37	0.49	-0.36	0.23	0.08	0.87	0.65	0.62		1.00	-0.07
Ni	-	-	-	-	-	-	-	-	-	-	-	-	-	-	-	-	-	-	1.00

Table 3. Pearson correlation matrix of physico-chemical parameters of groundwater

geogenic and anthropogenic source. The important contribution of lead (0.65) on F5 with their occurrence from Ait Ouyahia Iheddaden and Tala Hamza deposits to the sea area, highlight the contribution of naturel processes as leaching to lead appearance. During the high-water period F4 suggests that potassium fertilizers and home wastewater discharges are significant sources of K+, in addition the fifth factor accounts 7.57% of total variance and reveal the geogenic source of Manganese.

CONCLUSIONS

The present study represents the first and only research focused on the direct impact of Amizour's deposits associated to magmatic complex on the Soummam groundwater quality, by providing the needed informations to properly identify the nature and sources of pollution that threaten this vital resource through two different periods, high water and low water periods. We observed high concentrations of heavy metals in groundwater samples, the concentrations of Fe, Pb, Mn and Zn reach 17.75 mg/l, 6.99 mg/l, 6.46 mg/l, and 4.74 mg/l, respectively. Compared to the low-water period, the high-water campaign comprises more samples with values over the

detection limits, outlining significant weathering, transport and dilution of metals, notably Zn, Pb, Fe, Cd, Mn, and Ni caused by rainfall.

GIS-based modeling provided relevant maps exhibiting both temporal and spatial distribution of groundwater's physico-chemical properties, highlighting several localized contaminations within the study area. Furthermore, the Amizour's groundwater facies variability is mostly influenced by water-rock interaction mechanisms as the Gibbs diagram illustrates, with silicate mineral appearing as the region's predominant geological process.

Both geogenic and anthropogenic sources of pollution are revealed by statistical analysis applying PCA and a Pearson correlation matrix. The significant loading of cadmium (Cd) and nickel (Ni) on F2, as well as the strong correlation (r=0.97) between these metals during the high-water period confirm the impact of anthropogenic activities such as fertilizer's runoff. Furthermore, a moderate correlation between iron (Fe), zinc (Zn) and lead (Pb) indicates the geogenic pollution resulting from Amizour's deposits and water interactions.

The study highlights that the enrichment of iron (Fe), manganese (Mn) and cobalt (Co) during the high-water period is mainly geogenic, impacted by pH-influenced processes. This

localized enrichment near to Tala Hamza deposit, emphasize that their origin is primarily related to the silicate minerals weathering such as Pyroxene and Biotite from Miocene Igneous rocks as well as from Quartzite-sandstone of the Oligocene epoch, encased within pyroclastic breccias.

This work serves as a data bank for advancing sustainable development goals in the Amizour's region. It may also be regarded as a valuable reference on the baseline quality of Soummam groundwater quality prior to any potential influence by mining operations in the upcoming years.

REFERENCES

- Abraham, M., Dereje, F., Berihu, A. (2024). multivariate and water quality index approaches for spatial water quality assessment in Lake Ziway. Ethiopian Rift. Water Air Soil Pollution 235: 78.
- Assanaliev, B.S.G., Virchilo, V., Bitam, L. (1984). Carte géologique de B'eni Mansour, au 1/50 000, Entreprise Nationale de Recherche Mini`ere, Unité de Tizi Ouzou, Algérie. National Mining Research Enterprise, Tizi Ouzou Division, Algeria, Geological map of Beni Mansour, with a scale of 1:50,000.
- Balaji K, Janani N, Selvaperumal A, Ramachandaran J, Arthi T, Arunadevi K, Raviraj A. (2025). Geospatial assessment of groundwater quality in the Noyyal basin, Tamil Nadu, India using GIS and geostatistics. *Plant Science Today.* 12(2): 1–9. https://doi.org/10.14719/pst.6134
- Barkat, A., Bouaicha, F., Ziad, S., Mester, T., Sajtos, Z., Balla, D.,..., Szabó, G. (2023). The integrated use of heavy-metal pollution indices and the assessment of metallic health risks in the phreatic groundwater aquifer—The Case of the Oued Souf Valley in Algeria. *Hydrology*, 10(10), 201.
- Benabbes, D., Kessasra, F., Foughalia, A., Khemissa, Z., Kerouaz, M., Abdelloche, E. (2024). Coupled hydrogeological modeling and nitrate transport modeling in an anthropized valley, a case study of the lower Soummam valley (Bejaïa Northeast of Algeria) *Journal of African Earth Sciences 211*. https://doi.org/10.1016/j.jafrearsci.2024.105183
- Chaillou, G., Touchette, M., Buffin-Bélanger, T., Cloutier, C. A., Hétu, B., Roy, M. A. (2017). Hydrogeochemical evolution and groundwater mineralization of shallow aquifers in the Bas-Saint-Laurent region, Québec, Canada. *Canadian Water Resources Journal / Revue Canadienne Des Ressources Hydriques*, 43(2), 136–151. https://doi.org/10.1080/0 7011784.2017.1387817
- 7. Clinkx, C. (1973). Etude hydrogéologique de la nappe alluviale de la basse Soummam (Sidi-Aïch–Béjaïa)

- Rapport d'étude. Agence Nationale des Ressources Hydrauliques, Algérie (Hydrogeological study of the lower Soummam valley, between Sidi-Aïch and Bejaïa) Study report. National Hydraulic Resources Agency, Algeria). France. PhD. Thesis.
- 8. Davidson, W. (1993). Iron and manganese in lakes. *Earth-Science Reviews* 34, 119–163.
- 9. Fares, R., Naim, H., Bouadi, A. (2021). Groundwater pollution in the region of Relizane, Algeria with focus on the physical–chemical and bacteriological characteristics. *International Journal of Energy and Water Resources*, 5(3), 247–257.
- 10. General Compagny of Geophysics (C.G.G), (1970). Etude hydrogéologique par prospection électrique et sismique de la vallée de la Soummam (Tazmalt-Sidi-Aich). Compagnie Générale de Géophysique, Agence Nationale des Ressources Hydrauliques, Algérie (Hydrogeological study by electrical and seismic prospecting of the Soummam valley, between Tazmalt and Sidi-Aich. General Geophysical Company, National Hydraulic Resources Agency, Algeria).
- 11. Hao, W., Liu, H., Hao, S. et al. (2024). Characterization of heavy metal contamination in groundwater of typical mining area in Hunan Province. *Sci Rep 14*, 13054 https://doi.org/10.1038/s41598-024-63460-7
- 12. Hartmann, A., Goldscheider, N., Wagener, T., et al. (2014). Karst water resources in a changing world: Review of hydrological modeling approaches. *Reviews of Geophysics*, 52(3), 218–242.
- Hassissène, M. (1989). Etude géologique des Djebels Arbalou-Gouraya: éléments occidentaux du domaine des Babors (Région de Béjaia) Thèse Magistère U.S.T.H.B Alger.
- 14. ISO 5667-11:2009 Water quality Sampling Part 11: Guidance on sampling of groundwaters, Geneva.
- 15. ISO 5667-3:2018 Water quality Sampling- Part3: Preservation and handling of water samples, Geneva ISO.
- 16. ISO 5667-1:2020 Water quality. Sampling. Part 1: Guidance on the design of sampling programs and sampling techniques.
- 17. Jalali, M. (2009). Geochemistry characterization of groundwater in an agricultural area of Razan, Hamadan, Iran, *Environmental Earth Sciences* 56(7): 1479–1488. https://doi.org/10.1007/s00254-008-1245-9
- 18. Kessasra, F., Benabes, D., Seraoui, S., Chetibi, N., Mesbah, M., Khaled-Khodja, S., Foughalia, A. (2021). Groundwater flow and chloride transport modeling of the alluvial aquifer of lower Soummam Valley, Béjaia, North-East of Algeria, *Journal of African Earth Sciences* 173, January 2021, 104023. https://doi.org/10.1016/j.jafrearsci.2020.104023
- 19. Kumar, A., Krishna, A.P. (2021). Groundwater quality assessment using geospatial technique-based water quality index (WQI) approach in a coal mining

- region of India. *Arab J Geosci 14*, 1126. https://doi. org/10.1007/s12517-021-07474-9
- 20. Leikine, M.G.M., Semroud, B. (1988). Carte géologique d'Oued Amizour, au 1/50 000, Service géologique de l'Algérie, Algérie (Geological map of Oued Amizour, with a scale of 1:50,000. Algeria Geological Survey, Algeria.
- 21. Li, L., Li, W., Wang, Q. (2022). Prediction and zoning of the impact of underground coal mining on groundwater resources, *Process Safety and Environmental Protection*, *168*, 454–462. https://doi.org/10.1016/j.psep.2022.10.013
- 22. Medunić, G., Fiket, Ž., Ivanić, M. (2020). *Arsenic Contamination Status in Europe, Australia, and Other Parts of the World*. In: Srivastava, S. (eds) Arsenic in Drinking Water and Food. Springer, Singapore. https://doi.org/10.1007/978-981-13-8587-2 6
- 23. Olalekan, A. S., Adewoye, S. O., Sawyerr, H. O., Opasola, A. O., Raimi, M. L. (2023). Comprehensive understanding of hydrogeochemical evaluation of seasonal variability in groundwater quality dynamics in the gold mining areas of Osun State, Nigeria. *International Journal of Hydrology*, 7(5): 206–220. https://doi.org/10.15406/ijh.2023.07.00359
- 24. Ouyahia, N., Saou, A., Maza, M., Bouchraki, F. (2024). Evaluation of vulnerable zones to water pollution in the lower Soummam alluvial aquifer, Bejaia, Algeria. *Water Policy* 26(4): 321–335. https://doi.org/10.2166/wp.2024.120
- 25. Rashid, A., Ayub, M., Ullah, Z., Ali, A., Sardar, T., Iqbal, J., Gao, X., Bundschuh, J., Li, C., Khattak, S.A., et al. (2023). Groundwater quality, health risk assessment, and source distribution of heavy metals contamination around chromite mines: application of GIS, sustainable groundwater management, geostatistics, PCAMLR, and PMF receptor model. *Int. J. Environ. Res. Public Health* 20, 2113. https://doi.org/10.3390/ijerph20032113
- 26. Raza, S. et al. (2023). Effects of zinc-enriched amino acids on rice plants (*Oryza sativa* L.) for adaptation in saline-sodic soil conditions: growth, nutrient uptake and biofortification of zinc. *South. Afr. J. Bot.* 162, 370–380 https://doi.org/10.1016/j.sajb.2023.09.011
- 27. Saadali, B., Zerrouki, H., Drias, T., Khedidja, A., Belloula, M. (2022). Hydrogeochemical assessment

- to characterize the water quality for agricultural use in Mexanna and Bougous dams in the province of El Tarf, Algeria. *Environmental Earth Sciences*, *81*(5), 1–13. https://doi.org/10.1007/s12665-022-10185-0
- 28. Saadali, R., Dadachi, M. (2023). Comparative study of thevulnerability to groundwater pollution by the DRASTIC and SINTACS methods on the Amizour plain (Béjaia, North Algeria). *Earth Sci. Res. J. 27*, No. 4 (December, 2023): 381–389 https://doi:10.15446/esrj.v27n4.101618
- Ayon, S., Roy, D. K., Khan, R., Ornee, T.I., Goswami, S., Idris, A.M., Biswas P.K., Tamim, U. (2023).
 Provenance, weathering, climate and tectonic setting of Padma River sediments, Bangladesh: A geochemical approach, *CATENA*, 233, 107485, https://doi.org/10.1016/j.catena.2023.107485
- 30. Smida, H., Tarki, M., Dassi, L. (2022). Groundwater quality and mineralization process in the Braga shallow aquifer, Central Tunisia: an overview. *Carbonates Evaporites 37*, 28 https://doi.org/10.1007/s13146-022-00771-8
- 31. Saou, A., Maza, M., Jean Luc, S. (2012). Hydrochemical processes associated with double salinisation of water in an algerian aquifer, carbonated and evaporitic. *Pol. J. Environ. Stud.* 21(4), 1013–1024.
- 32. Semroud, B. (1981). Petrological evolution of the Neogene magmatic complex of the Béjaïa-Amizour region. doctoral thesis, Houari Boumediene University, Algiers.
- 33. Singha, S.S., Singha, S., Pasupuleti, S. et al. (2022). Knowledge-driven and machine learning decision tree-based approach for assessment of geospatial variation of groundwater quality around coal mining regions, Korba district, Central India. *Environ Earth Sci* 81, 36. https://doi.org/10.1007/s12665-021-10147-1
- 34. Thitame, S. N., Pondhe, G. M. (2010). Assessment of seasonal variation in physico-chemical characteristics and quality of Pravara River water for irrigation use in Sangamner, Dist Ahmednagar, Maharashtra. J. Chem. Pharm. Res, 2(2), 316–320.
- 35. Yao, L., Huo, Z., Feng, S. et al. (2014). Evaluation of spatial interpolation methods for groundwater level in an arid inland oasis, northwest China. *Environ Earth Sci* 71, 1911–1924. https://doi.org/10.1007/s12665-013-2595-5